Collective diffusivity in a sheared viscous emulsion: Effects of viscosity ratio

Abhilash Reddy Malipeddi and Kausik Sarkar

*Department of Mechanical and Aerospace Engineering, The George Washington University,
Washington, DC 20052, USA*

The shear-induced collective or gradient diffusivity in an emulsion of viscous drops, specifically as a function of viscosity ratio, was computed using a fully resolved numerical method. An initially randomly packed layer of viscous drops spreading due to drop-drop interactions in an imposed shear has been simulated. The collective diffusivity coefficient was computed using a self-similar solution of the drop concentration profile. We also obtained the collective diffusivity (the collective diffusivity coefficient multiplied by the average drop volume fraction), computing the dynamic structure factor from the simulated drop positions—an analysis typically applied only to homogeneous systems. The two quantities computed using entirely different methods are in broad agreement, including their predictions of nonmonotonic variations with increasing capillary number and viscosity ratio. The computed values were also found to match with past experimental measurements. The collective diffusivity coefficient computed here, as expected, is 1 order of magnitude larger than the self-diffusivity coefficient for a dilute emulsion previously computed using pairwise simulation of viscous drops in shear. The collective diffusivity coefficient computed here shows a nonmonotonic variation with viscosity ratio, in contrast to self-diffusivity computed using pairwise computation. The difference might point to an intrinsic difference in physics underlying the two diffusivities. Alternatively, it also might arise from drops not reaching equilibrium deformation in the period after one interaction and before the next—an effect absent in the pairwise simulation used for the computation of self-diffusivity. We offer a qualitative explanation of the nonmonotonic variation by relating it to average nonmonotonic drop deformation with increasing viscosity ratio. We also provide empirical correlations of the collective diffusivity as a function of viscosity ratio and capillary number.

I. INTRODUCTION

Noncolloidal particles in a sheared suspension or emulsion undergo a diffusive motion due to shear-induced hydrodynamic interactions between particles [1–5], which can be of great importance in chemical and biomedical flows. Specifically, for red blood cells (RBCs) in blood vessels at the physical hematocrit level of ∼45%, such shear-induced diffusion plays a critical role in determining their interactions and spatial concentrations [6,7]. Recently, we computed collective or gradient diffusivity in a concentrated viscous emulsion using fully resolved direct numerical simulation for a viscosity-matched system [8]. In this short article, we extend the analysis to emulsions where the drop viscosity differs from the matrix viscosity. Additional novelty of the work stems from an alternative means of computing collective diffusivity using dynamic structure factor theory in a nonhomogeneous system. The dynamic structure factor theory has previously been used only in homogeneous systems.

For a review of the literature of the shear-induced diffusion, we refer to our recent paper [8]. Briefly, shear-induced diffusion is characterized by self-diffusivity $D_s = \dot{\gamma} a^2 f_s(\phi)$ [$\dot{\gamma}$ is the shear

rate, a the particle radius, and $f_s(\phi)$ the nondimensional self-diffusivity, ϕ volume fraction], which defines the random motion of individual particles and is present even in a homogeneous suspension or emulsion, and collective or gradient diffusivity $D_c = \dot{\gamma} a^2 f_c(\phi)$ [$f_c(\phi)$ is the nondimensional collective diffusivity] that defines the diffusive flux $-D_c \nabla \phi$ in the presence of a concentration gradient [9]. Shear-induced self- and collective diffusion in rigid-sphere suspensions have been widely studied both experimentally [3,10] and numerically [11–15] since the pioneering work of Eckstein *et al.* [1]. However, emulsions of viscous drops in contrast have not been studied much. The first measurement of collective diffusivity in a viscous emulsion by King and Leighton [16] was marred by the presence of stabilizing surfactants and gave rise to values much smaller than theoretically expected. The only successful measurement of collective diffusivity in a viscous emulsion in the literature was performed by Hudson [17], who used more viscous drops to avoid emulsion instability. Self- and collective diffusivities in RBCs and vesicles have been measured in *in vitro* channels [6,7,18,19]. Self-diffusivity in a viscous emulsion has been measured using pair interactions between drops [4] in a dilute system, as well as using full-scale simulation in a nondilute system [20]. Pairwise simulation of vesicles [21,22] and RBCs [23] has been used to compute self-diffusivity in a dilute system of such complex rheological particles. Note that unlike self-diffusivity, collective diffusivity computation by summing pairwise displacement results in divergent integrals. Such problems could be addressed by a renormalization procedure using global constraints, as has been applied in analytical computation of effective stresses and sedimentation velocity in a rigid-sphere suspension [24,25].

In our previous article, we proposed a technique to compute collective diffusivity by numerically simulating a layer of initially closely packed drops diffusing in a plane shear. We used a front-tracking finite-difference method [26–29] to fully resolve each drop deforming and moving past each other. We obtained values for a nondimensional collective diffusivity coefficient that compared well with previous experiments [6,17]. Our simulation showed a nonmonotonic variation in collective diffusivity with capillary number where with increasing capillary number, initially the diffusivity increased, reached a maximum, and then subsequently decreased for larger values of capillary number. Although there was no other study of collective diffusivity versus capillary number in the literature, the self-diffusivity values computed using pairwise simulation by Loewenberg and Hinch [4] also showed a similar nonmonotonic trend.

Our previous study of a viscosity-matched system is extended here to systems where drop and matrix viscosities differ. Note that due to its ubiquitous presence in many chemical and biological phenomena and at the same time the difficulties in performing controlled experiments and the concomitant sparse literature to date, the shear-induced diffusion warrants further fundamental studies, such as the one attempted here, to delineate the nature of shear-induced diffusion. We have also developed a dynamic structure factor theory–based method to compute collective diffusivity. This method has so far been limited to homogeneous systems. Furthermore, the main result found here—the nonmonotonic variation of collective diffusivity with viscosity ratio, which offers an interesting contrast to the monotonic variation of self-diffusivity obtained previously using pairwise interactions [4]—*a posteriori* justifies the current study. We provide a detailed comparison with their pairwise drop trajectories to establish the accuracy of our simulation technique.

II. THEORETICAL FORMULATION

In this section, we provide the mathematical formulation and the numerical technique. The description here closely follows that of our previous article [8] and is presented here briefly for completeness. A layer of randomly packed drops of radius a and viscosity λ_d suspended in a fluid of viscosity λ_m is subjected to simple shear flow. Mathematically, the layer is infinite in the other two (x and z) directions. However, the computation, as described below, will be performed in a finite domain with periodic boundary conditions in these two directions and velocities prescribed at y boundaries to create the shear flow (Fig. 1). The results were examined to be independent of the
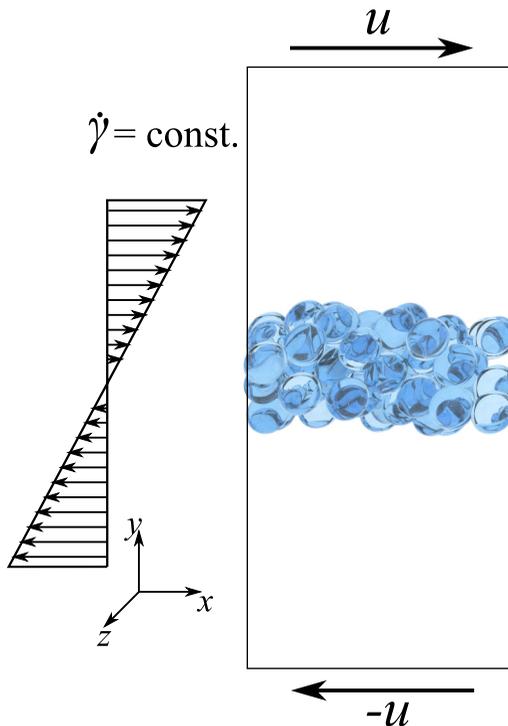
FIG. 1. A schematic of the layer of randomly placed drops in simple shear flow.

domain size [8]. The drops interact and move past each other, resulting in an effectively diffusive motion.

A. Gradient diffusivity from self-similar solution

The problem (it is homogeneous in the x and z directions) results in a diffusion equation for the local volume fraction, $\phi = \phi(y, t)$ in the y direction:

$$\frac{\partial \phi}{\partial t} = \frac{\partial}{\partial y}\left(D_c \frac{\partial \phi}{\partial y}\right), \tag{1}$$

with $D_c = \dot{\gamma}\phi a^2 f_2$ (assumption of two-particle interactions being dominant and thereby the rate of collision being $\dot{\gamma}\phi$) [4–6,30]. Here f_2 (subscript c for collective diffusivity $f_{c,2}$ has been dropped for convenience) is the nondimensional collective diffusivity in the velocity-gradient direction, the focus of the present work. The assumption of linear dependence of D_c on volume fraction, or equivalently, the dominance of pairwise interaction is *a posteriori* justified by the simulation results.

It has been shown by a detailed analysis that when a fixed number of particles spread due to shear-induced diffusion, Eq. (1), nondimensionalized using $t = t'/\dot{\gamma}$, $y = y'a$ admits a self-similar parabolic concentration [6]

$$\psi(\eta) = (f_2 t')^{1/3}\phi = (b - \eta^2/6), \quad \eta = y'/(f_2 t')^{1/3}, \tag{2}$$

in the similarity variable η (b is a free parameter). Note the $t^{1/3}$ spread of the profile in contrast to $t^{1/2}$ growth in systems with a constant diffusivity D_c (i.e., independent of volume fraction). Note that in the case of particles spreading from one side in an initially Heaviside concentration profile [30], the characteristic exponent is still 1/2, even when $D_c = \dot{\gamma}\phi^m a^2 f_2$ with $m > 1$. It can be shown
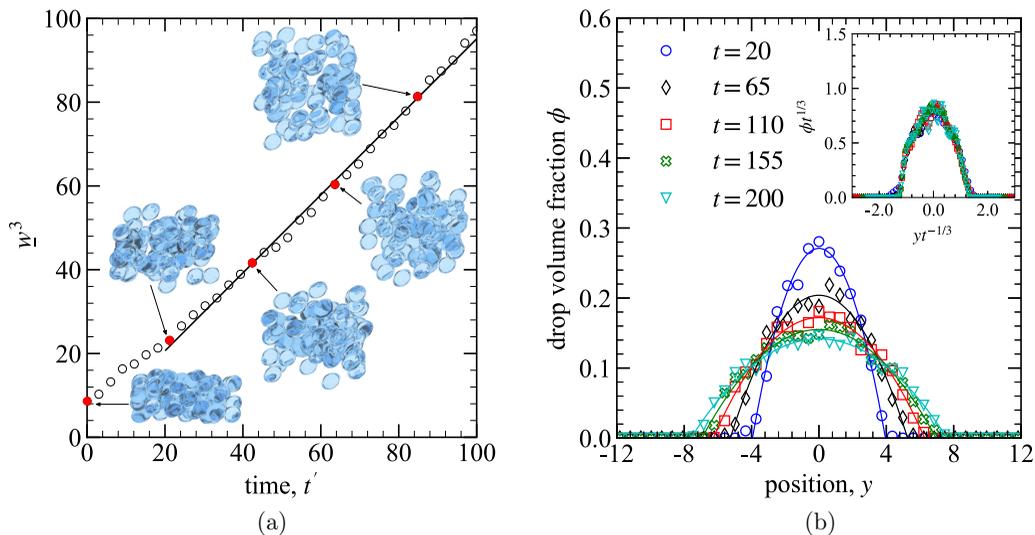
FIG. 2. (a) Cube of the width of the layer of drops plotted as a function of time grows linearly with time. Snapshots of the evolving drop configurations at various time instants. See Supplemental Material [31] for a movie of drop evolution. (b) Concentration profile of the drops at various time instants, showing a parabolic profile broadening with time. Inset shows a collapse of the same when plotted against the scaled similarity variable according to Eq. (2).

[6] that according to (2), the half-width $\underline{w}$ of the $\phi(y')$ profile at half-height satisfies

$$\underline{w}^3 - \underline{w}_o^3 = Kt', \quad K = 9f_2N_0/(4\sqrt{2}), \quad N_o = \int \phi(y', t') \, dy'. \tag{3}$$

Here $\underline{w}_0$ is the initial width, and N_o is a conserved quantity related to the particular nature of the problem mentioned before—a fixed number of particles diffusing out. f_2 is computed by fitting a parabolic curve for the droplet concentration at any instant of time and obtaining the half-width $\underline{w}(t')$. Figure 2(a) shows the linear growth of $\underline{w}^2$ past $t' \sim 20$. Figure 2(b) shows that the volume fraction of the drops follows a parabolic spatial distribution at different time instants, all of them collapsing to a single curve in the similarity variable [inset of Fig. 2(b)] consistent with (2). In Malipeddi and Sarkar [8], we also proposed and developed an alternative method that avoids curve fitting and computes the standard deviation, called "modified" width, of the concentration profile from the drop positions (y'_i) as

$$w = \sqrt{\frac{1}{N}\sum_{i=1}^{N}(y'_i - \mu)^2}, \quad \mu = \frac{1}{N}\sum_{i=1}^{N}y'_i. \tag{4}$$

Similar to Eq. (3), the cube of the modified width w^3 scales linearly with time, albeit with a slightly different constant,

$$w^3 - w_o^3 = K't', \quad K' = 9f_2N_0/(10\sqrt{5}). \tag{5}$$

In Malipeddi and Sarkar [8] we showed that the two procedures gave rise to identical values within statistical variations intrinsic to the system. Here, we use Eq. (5) to obtain the value of the collective diffusivity f_2. Each simulation is run till $t' = 200$. We discard the data in the initial transient region before the self-similar profile is reached ($t' < 20$). The remaining portion of the data is split into four smaller intervals of 45 inverse shear units. The length of these intervals is enough to ensure

that the drop movements in each interval are uncorrelated. The slope of $w^3 - w_o^3$ vs time for each subinterval is calculated and the mean value of these is reported. The standard deviation of the value across these subintervals is used to estimate the uncertainty in the measurement.

B. Gradient diffusivity from dynamic structure factor

Both self- and collective diffusivities can also be computed from particle dynamics in a homogeneous system [9,13]. The computation of collective or gradient diffusivity—which measures diffusion down a concentration gradient—in a homogeneous system is counterintuitive; it is predicated on the analysis of the decay of the spontaneously arising stochastic fluctuations encapsulated in the wave-number-dependent dynamic structure factor. Originally the theory stemmed from computation of diffusivity from dynamic light scattering (DLS), where a scattered response of a monochromatic beam of laser from a scattering volume containing multiple scatterers (large macromolecules such as DNA, proteins, amino acids, viruses, and bacteria) is measured [32]. For a dilute system of noninteracting scatterers, the autocorrelation of the fluctuation decays exponentially and the decay time is inversely proportional to the diffusivity. For concentrated systems, hydrodynamic interactions between the fluctuating particles cannot be neglected and the measured scattered response requires careful analysis [33–35] and proper interpretation. In different limits it reduces to collective or self-diffusivity [9]. Leshansky and Brady [14] carefully described the theory and applied it to shear-induced diffusion. The analysis assumes no coalescence or breakup, as was also true for our simulation.

The scattered response at wave number $\mathbf{k}$(nondimensionalized by a) from N scatterers located at $\mathbf{x}'_\alpha(t'), \alpha = 1, 2, ...N$ is proportional to the intermediate scattering function

$$F(\mathbf{k}, t') = \frac{1}{N}\left\langle \sum_{\alpha, \beta=1}^{N} e^{i\mathbf{k}\cdot[\mathbf{x}'_\alpha(t')-\mathbf{x}'_\beta(0)]} \right\rangle. \tag{6}$$

Note that using the property of the Dirac δ function, the number density of the scatterers (here droplets) and its spatial Fourier transform can be written as

$$n(\mathbf{x}', t') = \sum_{\alpha=1}^{N} \delta(\mathbf{x}' - \mathbf{x}'_\alpha), \quad \hat{n}(\mathbf{k}, t') = \sum_{\alpha=1}^{N} e^{i\mathbf{k}\cdot\mathbf{x}'_\alpha}. \tag{7}$$

Therefore, $F(\mathbf{k}, t') = 1/N\langle\hat{n}(\mathbf{k}, t')\hat{n}^*(\mathbf{k}, 0)\rangle$ may be regarded as measuring the autocorrelation of the fluctuation $n'(\mathbf{x}', t')$ [where $n(\mathbf{x}', t) = n_0 + n'(\mathbf{x}', t')$] at wave number $\mathbf{k}$ for a statistically homogeneous system, as the constant background n_0 would not contribute to the autocorrelation. The system is not homogeneous but evolves from a nonhomogeneous initial condition. Leshansky and Brady [14] showed that the number density satisfies an advection diffusion equation in a shear flow $\mathbf{U} + \dot{\mathbf{\Gamma}} \cdot \mathbf{x}$ ($\mathbf{U}$ is the average flow and $\dot{\mathbf{\Gamma}}$ is the velocity-gradient tensor):

$$\frac{\partial n}{\partial t} + (\mathbf{U} + \dot{\mathbf{\Gamma}} \cdot \mathbf{x}) \cdot \nabla n = \mathbf{D}^c\nabla^2 n. \tag{8}$$

In spite of the advection terms in Eq. (8), in a simple shear due to the orthogonality of the $\mathbf{k}(=k\hat{\mathbf{y}})$ vector to the velocity field one obtains a simple relation for the diffusivity in the gradient direction [14]:

$$D_{yy}^c = -\frac{1}{k^2}\frac{d(\ln F)}{dt'}. \tag{9}$$

C. Direct numerical simulation

We solve the incompressible Navier-Stokes equations using a front-tracking method [26,27]:

$$\nabla \cdot \mathbf{u} = 0, \quad \frac{\partial(\rho \mathbf{u})}{\partial t} + \nabla \cdot (\rho \mathbf{u} \mathbf{u}) = -\nabla p + \nabla \cdot [\mu \{\nabla \mathbf{u} + (\nabla \mathbf{u})^T\}] - \int_{\partial B} \kappa \mathbf{n} \sigma \delta(\mathbf{x} - \mathbf{x}') dS(\mathbf{x}').$$

(10)

Here $\mathbf{u}$, p, ρ, and μ are the velocity, pressure, density, and viscosity, respectively. κ is the local drop surface curvature, $\mathbf{n}$ is the unit outward normal to the surface ∂B of all drops, and σ is the interfacial tension. In this numerical method, all drops and their interactions are resolved. The method has been used by our group in many problems involving drops [27,36,37] and capsules [38–40] in viscous and viscoelastic fluids [41–48]. Here, a uniform shear flow is generated in a computational domain, which is periodic in the x and z directions and has numerical walls in the y direction moving with specified velocities (Fig. 1). The distance between the walls is $L_y = 28a$ (a is the drop radius), sufficiently large to simulate an unbounded shear. The length of the domain in the x and z directions is $L_x = L_z = 14a$. A $96 \times 192 \times 96$ uniform grid is used in the computational domain, leading to 15 grid points per drop diameter, shown to be sufficient in our earlier studies. In our previous article [8], we carefully varied the domain lengths to ensure that the results are independent of them. There we also showed that the results did not change with drop numbers above 70 or with volume fraction corresponding to $N_0(=1.43$ here) beyond a value. Note that the volume fraction and N_0 are related by (3). The simulations here are executed with 70 drops and an initial volume fraction of 45%. As noted in [8], the explicit nature of the code restricts the simulation to a small but nonzero $\mathrm{Re} = \rho \dot{\gamma} a^2/\mu = 0.1$, which has been shown to match Stokes flow results [29]. In Fig. 5 below, we will show that the approach matches boundary element simulation of a Stokes flow.

III. RESULTS AND DISCUSSION

A. Effects of viscosity ratio variation

We calculate the collective diffusivity coefficient f_2 for a range of viscosity ratios using the self-similar scaling of the drop layer width. We also compute the collective diffusivity itself D_{yy}^c using the wave-number-dependent dynamic structure factor (DSF).

1. f_2 from scaling of the layer width

Figure 3 shows the growth of the width of the drop layer with time for different viscosity ratios at Ca $= 0.05$ [Fig. 3(a)] and Ca $= 0.30$ [Fig. 3(b)], displaying clearly a 1/3 scaling of the layer width with time. From the slopes, f_2 is computed according to Eq. (3) and plotted in Fig. 4(a). As can be expected from Fig. 3, slope varies nonmonotonically with λ_μ [Fig. 4(a)]: f_2 increases initially with increasing λ_μ and reaches a maximum around the viscosity ratio of about 1, and then decreases. At higher viscosity ratios, drop deformation is known to decrease, reaching the limit of a rigid sphere, thereby resulting in lower diffusivity. In fact, due to reversibility of the Stokes flow, pairwise interaction fails to produce any diffusive motion in the rigid-particle limit. In a rigid-sphere suspension, $D_{yy} \sim \phi^2$ in the leading order [5], and therefore $f_2 = 0$.

Note that we found a nonmonotonic variation f_2 with Ca previously [8]. Similar to the case there, the reason for the nonmonotonic behavior is the drop geometry as a function of λ_μ. In Fig. 4(b), we compute drop deformation characterized by Taylor deformation $D = (L - B)/(L + B)$ [L being the maximum distance of the drop interface from its center and the B being the minimum distance] [49], averaged over all drops, once it reaches a steady value after initial transients. It shows that with increasing λ_μ, D first increases, increase roughly coinciding with the region where f_2 also increases, and then decreases. At the same time the drop inclination angle φ, also plotted in Fig. 4(b), with the flow direction steadily decreases. The increasing trend of D and the variation of φ are consistent with the small deformation moderate λ_μ perturbative results $D = Ca(19\lambda + 16)/(16\lambda + 16)$ [49] and $\theta = \pi/4 - Ca(2\lambda + 3)(19\lambda + 16)/(80\lambda + 80)$ [50]. (As is well recognized in the literature,
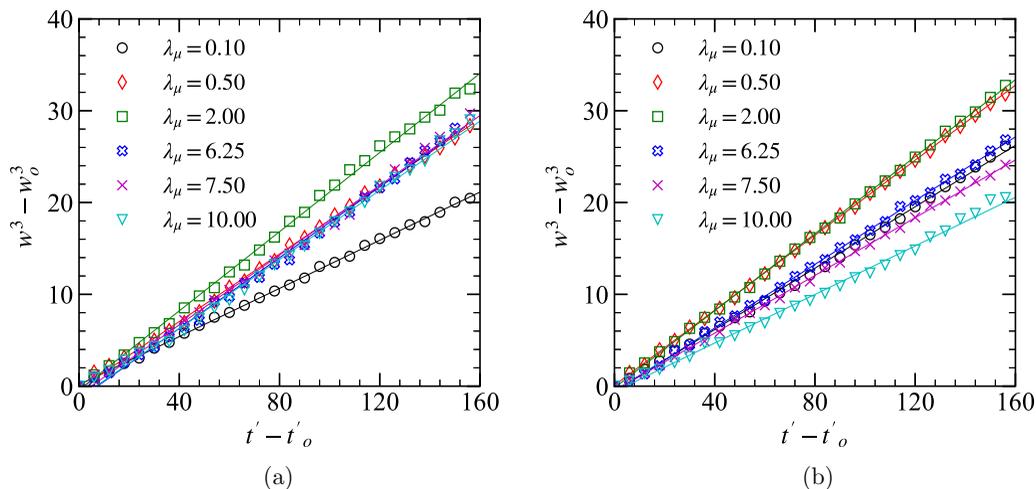
FIG. 3. Cube of width of the drop layer vs time for various viscosity ratios for Ca = 0.05(a) and Ca = 0.30(b) showing the expected linear trend.

the analytical result fails to predict the decreasing trend of D at higher viscosity ratio.) The initially increasing drop deformation increases the hindrance to passage of drops past each other, increasing the diffusivity coefficient f_2. Subsequently, the decreasing deformation as well as decreasing inclination angle facilitates drops passing each other, reducing f_2. Note that Rusconi and Stone [30] have shown that the geometry of the suspended particles can have significant effects on gradient diffusivity, e.g., highly asymmetric platelike particles have gradient diffusivity 2 orders of magnitude higher than that of rigid spheres at similar volume fraction.

We find the collective diffusivity coefficient computed here as well as in our previous paper [8] to be consistently 8–9 times higher than those computed using a simulation of pair interactions between drops for a dilute emulsion by Loewenberg and Hinch [4]. This ratio is similar to what was found for rough sphere suspensions—ratio of collective diffusivity to self-diffusivity is ∼6 [5]. As noted before, Loewenberg and Hinch [4] found self-diffusivity to vary nonmonotonically with increasing Ca as did we [8] (also see below). However, their self-diffusivity coefficient $f_{s,2}$
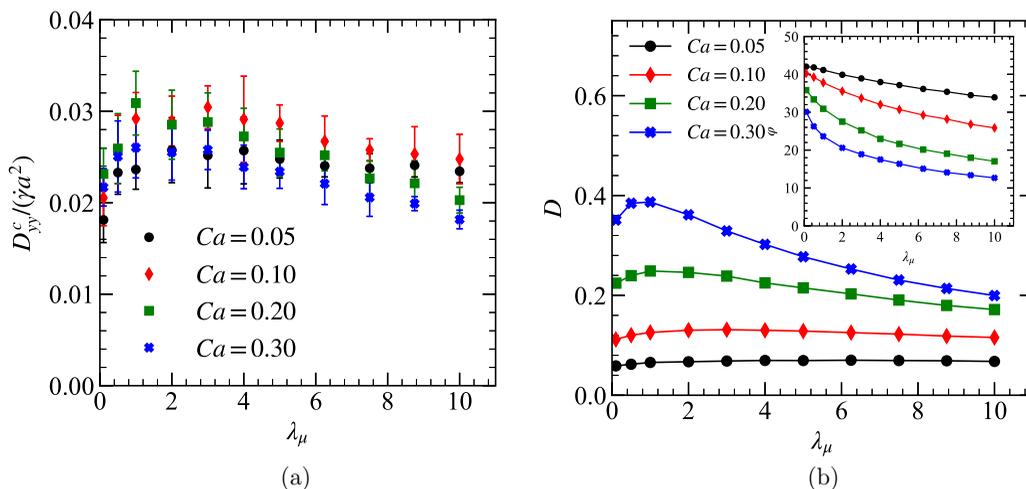

FIG. 4. (a) Dimensionless coefficient of diffusion f_2 vs viscosity ratio λ_μ for different capillary numbers. (b) Main figure shows mean drop deformation parameter and inset shows drop orientation angle.
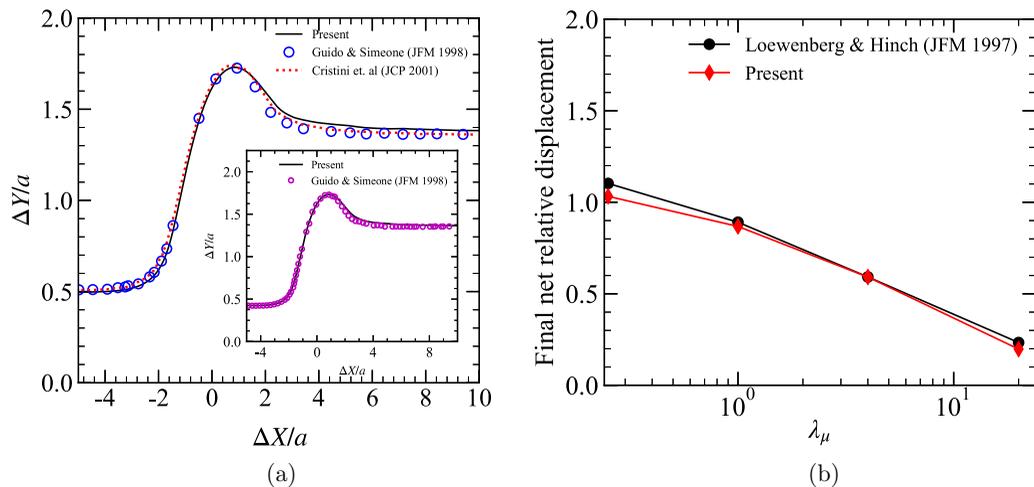
FIG. 5. (a) Relative displacement of two drops interacting in shear flow comparing our results (solid line) with those obtained from boundary element method (dotted line) by Cristini *et al.* [52] and experimental measurements (open circles) by Guido and Simeone [51]. Main figure is with $Ca = 0.135$, $\lambda_\mu = 1.37$. Inset is with $Ca = 0.13$ and $\lambda_\mu = 1.4$. (b) Final net relative displacement of two drops, initially separated $0.5a$ in the gradient direction for different viscosity ratios λ_μ at $Ca = 0.30$. Present results (diamonds) compare reasonably well with boundary element method results of Loewenberg and Hinch [4].

did not show a nonmonotonic variation with λ_μ; it showed a constant variation for the small λ_μ and then a strictly monotonic decay for larger values of λ_μ. Using an identical approach of simulating pair interactions, Omori *et al.* [23] computed the self-diffusivity of a dilute suspension of red blood cells to find a monotonically decreasing value for $f_{s,2}$. Note, however, that the self- and gradient diffusivities, although both are generated by the same shear-induced irreversible drop-drop interactions, describe manifestly different aspects of emulsion behaviors and could have different trends. Although the current work focuses on collective diffusivity, we compare here our simulation method with that of Loewenberg and Hinch [4]. Computing self-diffusivity by simulating pair interactions between droplets using their method would require a single set of parameters $\sim$60–70 simulations with different relative initial positions of the droplets. It would be computationally expensive, onerous, and is clearly outside the scope of the present work. Here we compute pair interactions for droplets in shear to show in Fig. 5(b) that the final net relative displacement [initially at (0,0,0) and $(-10a, 0.5a, 0)$] as a function of viscosity ratio matches identically with the boundary element simulations of Loewenberg and Hinch [4]. In Fig. 5(a), the relative y displacement between drops as a function of relative x displacement for two different capillary numbers also offers excellent match with experiments [51], as well as more recent boundary element simulation from the same group Cristini *et al.* [52]. Successful comparison with previous methods offers validation for our methods, specifically for our numerical simulation technique. It remains difficult to conclusively argue for a simple physical reason for the trend in effective properties of overall emulsions such as gradient or self-diffusivities. However, the monotonic decrease of final relative displacement in Fig. 5(b) offers a plausible reason for monotonically decreasing self-diffusivity in a dilute emulsion, i.e., neglecting more than two-particle interaction, as seen in Loewenberg and Hinch [4].

2. $D_{yy}^c / \dot{\gamma} a^2$ using dynamic structure factor

We compute $F(\mathbf{k}, t')$ using (6) from the drop positions (discarding initial data $t' = 20$). The resulting intermediate scattering functions are averaged over overlapping intervals to obtain a smooth time evolution curve [14]. Figure 6(a) shows that $-\ln F(\mathbf{k}, t')/k^2$ at $Ca = 0.20$ and $\lambda_\mu = 5.0$ for different wave numbers normalized by their initial value displays a linear growth
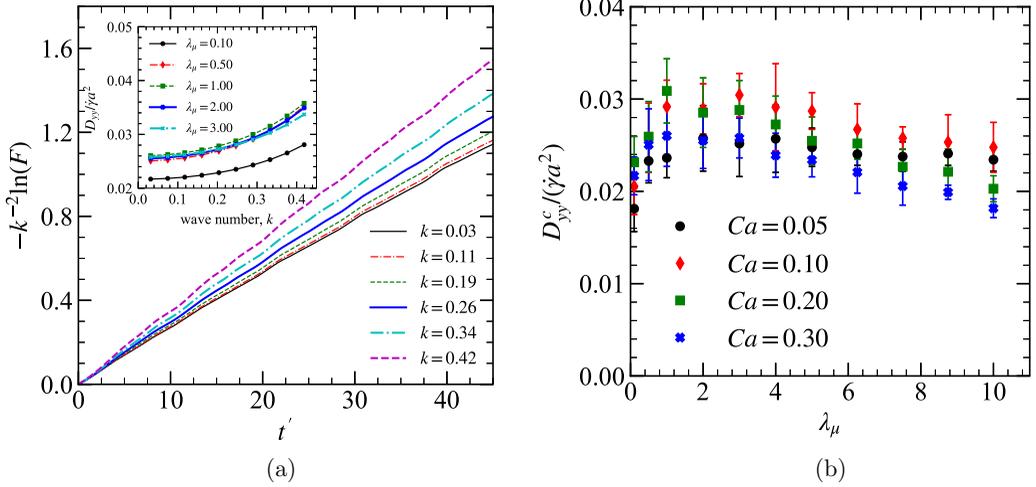
FIG. 6. (a) Main figure shows the linear growth in $-\ln F(\mathbf{k}, t')/k^2$ with time for various wave numbers for Ca = 0.20 and $\lambda_\mu = 5.0$. Inset shows $D^c_{yy}/\dot\gamma a^2$ vs wave number k for a few different viscosity ratios. (b) $D^c_{yy}/\dot\gamma a^2$ vs viscosity ratio for different Ca values.

with the slope being asymptotic to a single value in the limit of $k \to 0$ or the large wavelength limit. This limiting slope, $D_{c,yy}$, is plotted as a function of λ_μ for several Ca values in Fig. 6(b). The trend is remarkably similar to that of f_2 vs λ_μ in Fig. 4(a). A direct comparison is not available, as the emulsion is not homogeneous and the average concentration of the progressively widening drop layer decreases with time. However, note that the ratio $D^c_{yy}/f_2 \sim 0.1$ is close to an average volume fraction φ over the whole diffusive process starting with the maximum $\varphi_{\text{initial}} \sim 0.25$ for the post-transient initial packed layer at $t' = 20$. We plot in the inset of Fig. 6(a) the slope of $-\ln F/k^2$ as a function of wave number k for different λ_μ. However, a straightforward interpretation of this quantity as the wave-number-dependent diffusivity is not possible as is done in the literature [14] because of the inhomogeneous nature of the problem. Here the process is dominated by an initial inhomogeneous distribution containing a finite concentration gradient relaxing through a nonlinear diffusive process [Eq. (1)], unlike the typical case in the literature where it is a spontaneously arising infinitesimal stochastic concentration fluctuation relaxing. As a result, the slope increases with k, unlike, say, in Leshansky and Brady [14] where it decreases, reaching self-diffusivity in the limit of $k \to \infty$. However, we note that the dynamic structure factor, which was typically computed and applied only to homogeneous systems, offers a novel perspective about the gradient diffusivity of nonhomogeneous systems. Finally, the remarkable similarity of the curves in Figs. 4(a) and 6(b), despite the completely independent way of computing them, makes us confident about the trends of variations of f_2 as well as D^c_{yy}.

B. Effects of capillary number variation

Figure 7(a) plots f_2 vs Ca for three different viscosity ratios, all showing the nonmonotonic variation. As noted in [8], the nonmonotonicity arises from the competition between rising deformation and decreasing inclination with increasing Ca [shown in Fig. 7(b)], the former increasing diffusivity initially and the latter eventually dominating to decrease it. Note that as we noted in [8], a slightly different explanation was offered by Loewenberg and Hinch [4] for the nonmonotonic variation of the self-diffusivity coefficient $f_{s,2}$ with Ca. In Fig. 7(c), we also plot D^c_{yy} as a function of Ca for the same three λ_μ values. It shows again very similar trends as in Fig. 7(a). Note that the values found here are in agreement with the experimental measurement of Hudson [17], who performed the experiments for viscosity ratios of 0.17–0.19 (depending on the drop liquids),
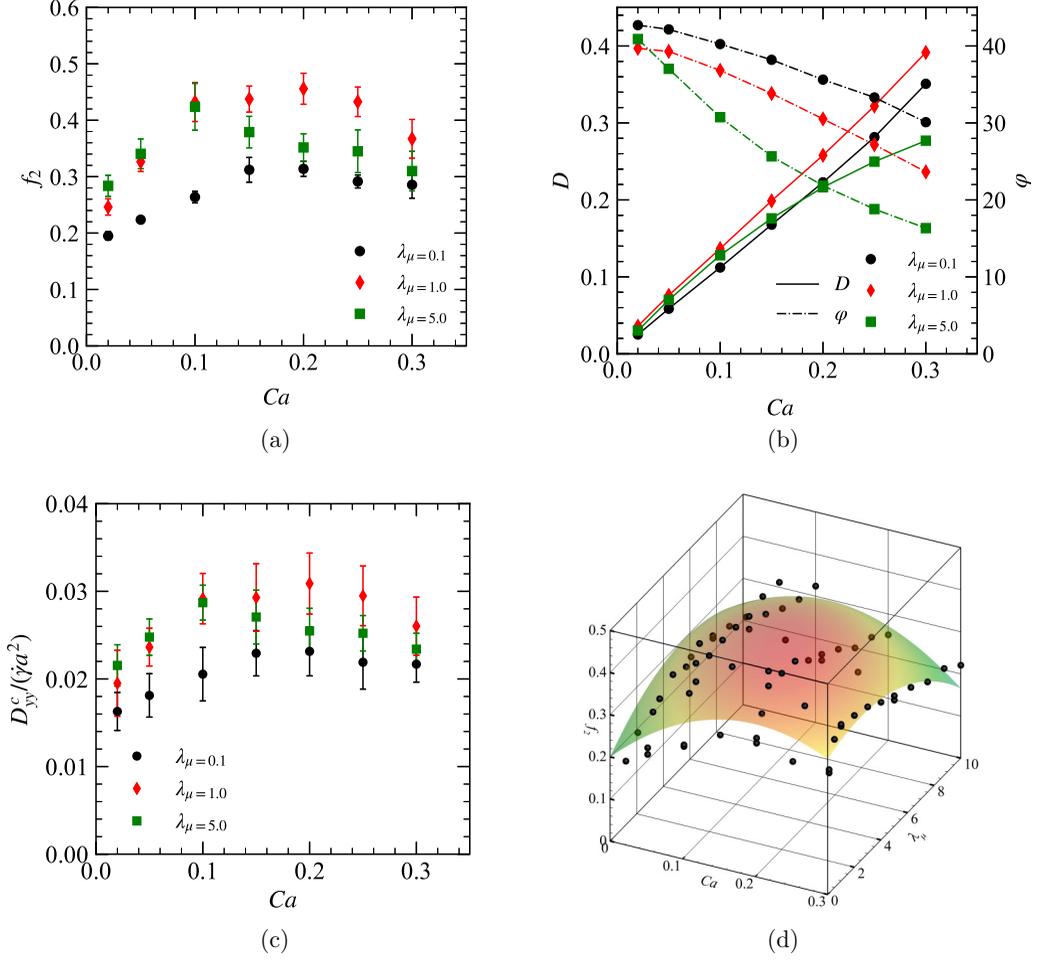
FIG. 7. (a) Dimensionless gradient diffusivity f_2 and (b) average drop deformation parameter, orientation angle vs Ca for different viscosity ratios. (c) $D_{yy}^c/\dot{\gamma}a^2$ vs Ca for different viscosity ratios. (d) Surface plot showing f_2 as a function of capillary number Ca and viscosity ratio λ_μ. The correlation describing the surface is given in Eq. (9).

obtaining $f_2 = 0.16$–0.25 for Ca of 0.02–0.40. Grandchamp *et al.* [6] measured a value of ~ 0.77 (rescaled by particle volume) for red blood cells.

Finally, by combining all the results from the previous sections, we have generated an empirical correlation for the dimensionless diffusivity f_2 as a function of capillary number and viscosity ratio:

$$f_2 = -4.06\text{Ca}^2 + 3.12 \times 10^{-3}\lambda_\mu^2 - 6.52 \times 10^{-2}\text{Ca}\lambda_\mu + 1.62\text{Ca} + 3.52 \times 10^{-2}\lambda_\mu + 0.2. \quad (11)$$

The empirical correlation is plotted in Fig. 7(d). Similarly, an empirical correlation for $D_{yy}^c/\dot{\gamma}a^2$ is also obtained [not plotted, as the variation is similar to Fig. 7(d)]:

$$D_{yy}^c/\dot{\gamma}a^2 = \big(-2.36\text{Ca}^2 - 1.67 \times 10^{-3}\lambda_\mu^2 - 3.88 \times 10^{-2}\text{Ca}\lambda_\mu$$
$$+ 0.94\text{Ca} + 1.86 \times 10^{-2}\lambda_\mu + 0.17\big)/10. \quad (12)$$

IV. CONCLUSION

We have computed the shear-induced gradient diffusivity in a sheared viscous emulsion of droplets using a front-tracking-based direct numerical simulation. We simulated the deformation and motion of droplets initially packed in a layer subjected to a simple shear. We focused on the effects of the varying viscosity ratio between the drop and matrix fluids. From the time evolution of the droplet phase concentration, we compute the coefficient f_2 of the gradient or collective diffusivity using a self-similar solution of the one-dimensional nonlinear diffusion equation assumed to be satisfied by the system. There has not been any prior numerical computation of the quantity in the literature for emulsion of viscous drops, capsules, or vesicles. There has been one experimental measurement of this quantity for viscous emulsion in the literature, which is in agreement with the values computed here. It is also of the same order as what has been measured in suspensions of cells and vesicles.

The computed coefficient varied nonmonotonically with the viscosity ratio—in the range of viscosity ratio $[0.1, \sim 2]$ gradient diffusivity increased with viscosity ratio and decreases for values beyond this range. The nonmonotonic behavior arises due to nonmonotonic variation in drop deformation with viscosity ratio. The nonmonotonic trend is slightly different from that computed for self-diffusivity computed in the literature using pair interactions for both viscous droplets [4]—the self-diffusivity coefficient remained constant for smaller viscosity ratios decreasing monotonically at higher viscosity ratios—and capsules [23]—monotonically decreasing with the viscosity ratio. We validated our computational technique against the boundary element technique used by those authors. This led us to believe that the nonmonotonic behavior results from multiparticle interactions, or self and gradient diffusivities have different variations with viscosity ratio at low viscosity ratio, an issue to be explored in future work.

We also compute the gradient diffusivity D_{yy}^c by computing the dynamic structure factor, a computation that has so far been restricted to homogeneous suspension. The results when appropriately scaled with average volume fraction are in agreement with the computed f_2 values, and more importantly, they show very similar variation with viscosity ratio, although the two methodologies are very different. Based on the simulation results, we offer two phenomenological correlations for f_2 and D_{yy}^c as functions of capillary number and viscosity ratio.

[1] E. C. Eckstein, D. G. Bailey, and A. H. Shapiro, Self-diffusion of particles in shear flow of a suspension, J. Fluid Mech. **79**, 191 (1977).

[2] R. H. Davis, Hydrodynamic diffusion of suspended particles: A symposium, J. Fluid Mech. **310**, 325 (1996).

[3] D. T. Leighton and A. Acrivos, Measurement of shear-induced self-diffusion in concentrated suspensions of spheres, J. Fluid Mech. **177**, 109 (1987).

[4] M. Loewenberg and E. J. Hinch, Collision of two deformable drops in shear flow, J. Fluid Mech. **338**, 299 (1997).

[5] F. da Cunha and E. J. Hinch, Shear-induced dispersion in a dilute suspension of rough spheres, J. Fluid Mech. **309**, 211 (1996).

[6] X. Grandchamp, G. Coupier, A. Srivastav, C. Minetti, and T. Podgorski, Lift and Down-Gradient Shear-Induced Diffusion in Red Blood Cell Suspensions, Phys. Rev. Lett. **110**, 108101 (2013).

[7] L. Bureau, G. Coupier, F. Dubois, A. Duperray, A. Farutin, C. Minetti, C. Misbah, T. Podgorski, D. Tsvirkun, and M. Vysokikh, Blood flow and microgravity, C. R. Mec. **345**, 78 (2017).

[8] A. R. Malipeddi and K. Sarkar, Shear-induced collective diffusivity down a concentration gradient in a viscous emulsion of drops, J. Fluid Mech. **868**, 5 (2019).

[9] J. M. Rallison and E. J. Hinch, The effect of particle interactions on dynamic light scattering from a dilute suspension, J. Fluid Mech. **167**, 131 (1986).

[10] L. V. A. Breedveld, Shear-induced self-diffusion in concentrated suspensions, Ph.D. thesis, University of Twente, 2000.

[11] A. Sierou and J. F. Brady, Shear-induced self-diffusion in non-colloidal suspensions, J. Fluid Mech. **506**, 285 (2004).

[12] M. Marchioro and A. Acrivos, Shear-induced particle diffusivities from numerical simulations, J. Fluid Mech. **443**, 101 (2001).

[13] J. F. Morris and J. F. Brady, Self-diffusion in sheared suspensions, J. Fluid Mech. **312**, 223 (1996).

[14] A. M. Leshansky and J. F. Brady, Dynamic structure factor study of diffusion in strongly sheared suspensions, J. Fluid Mech. **527**, 141 (2005).

[15] A. M. Leshansky, J. F. Morris, and J. F. Brady, Collective diffusion in sheared colloidal suspensions, J. Fluid Mech. **597**, 305 (2008).

[16] M. R. King and D. T. Leighton, Measurement of shear-induced dispersion in a dilute emulsion, Phys. Fluids **13**, 397 (2001).

[17] S. D. Hudson, Wall migration and shear-induced diffusion of fluid droplets in emulsions, Phys. Fluids **15**, 1106 (2003).

[18] J. M. Higgins, D. T. Eddington, S. N. Bhatia, and L. Mahadevan, Statistical dynamics of flowing red blood cells by morphological image processing, PLOS Comput. Biol. **5**, e1000288 (2009).

[19] H. L. Goldsmith and J. C. Marlow, Flow behavior of erythrocytes, II. Particle motions in concentrated suspensions of ghost cells, J. Colloid Interface Sci. **71**, 383 (1979).

[20] M. H.-Y. Tan, D.-V. Le, and K.-H. Chiam, Hydrodynamic diffusion of a suspension of elastic capsules in bounded simple shear flow, Soft Matter **8**, 2243 (2012).

[21] H. Zhao and E. S. G. Shaqfeh, The dynamics of a non-dilute vesicle suspension in a simple shear flow, J. Fluid Mech. **725**, 709 (2013).

[22] P.-Y. Gires, A. Srivastav, C. Misbah, T. Podgorski, and G. Coupier, Pairwise hydrodynamic interactions and diffusion in a vesicle suspension, Phys. Fluids **26**, 013304 (2014).

[23] T. Omori, T. Ishikawa, Y. Imai, and T. Yamaguchi, Shear-induced diffusion of red blood cells in a semi-dilute suspension, J. Fluid Mech. **724**, 154 (2013).

[24] G. K. Batchelor, Sedimentation in a dilute dispersion of spheres, J. Fluid Mech. **52**, 245 (1972).

[25] G. K. Batchelor and J. T. Green, Determination of bulk stress in a suspension of spherical-particles to order C-2, J. Fluid Mech. **56**, 401 (1972).

[26] G. Tryggvason, B. Bunner, A. Esmaeeli, D. Juric, N. Al-Rawahi, W. Tauber, J. Han, S. Nas, and Y.-J. Jan, A front-tracking method for the computations of multiphase flow, J. Comput. Phys. **169**, 708 (2001).

[27] K. Sarkar and W. R. Schowalter, Deformation of a two-dimensional drop at non-zero Reynolds number in time-periodic extensional flows: Numerical simulation, J. Fluid Mech. **436**, 177 (2001).

[28] X. Y. Li and K. Sarkar, Drop dynamics in an oscillating extensional flow at finite Reynolds numbers, Phys. Fluids **17**, 027103 (2005).

[29] P. Srivastava, A. R. Malipeddi, and K. Sarkar, Steady shear rheology of a viscous emulsion in the presence of finite inertia at moderate volume fractions: Sign reversal of normal stress differences, J. Fluid Mech. **805**, 494 (2016).

[30] R. Rusconi and H. A. Stone, Shear-Induced Diffusion of Platelike Particles in Microchannels, Phys. Rev. Lett. **101**, 254502 (2008).

[31] See Supplemental Material at http://link.aps.org/supplemental/10.1103/PhysRevFluids.4.093603 for a movie showing the evolution of the layer of drops.

[32] B. J. Berne and R. Pecora, *Dynamic Light Scattering: With Applications to Chemistry, Biology, and Physics* (Dover Publications, Mineola, NY, 2000).

[33] A. R. Altenberger, On the wave vector dependent mutual diffusion of interacting Brownian particles, J. Chem. Phys. **70**, 1994 (1979).

[34] W. B. Russel and A. B. Glendinning, The effective diffusion coefficient detected by dynamic light scattering, J. Chem. Phys. **74**, 948 (1981).

[35] A. R. Altenberger and J. M. Deutch, Light scattering from dilute macromolecular solutions, J. Chem. Phys. **59**, 894 (1973).

[36] X. Li and K. Sarkar, Effects of inertia on the rheology of a dilute emulsion of drops in shear, J. Rheol. **49**, 1377 (2005).

[37] X. Li and K. Sarkar, Negative Normal Stress Elasticity of Emulsions of Viscous Drops at Finite Inertia, Phys. Rev. Lett. **95**, 256001(2005).

[38] X. Li and K. Sarkar, Front tracking simulation of deformation and buckling instability of a liquid capsule enclosed by an elastic membrane, J. Comput. Phys. **227**, 4998 (2008).

[39] R. K. Singh, X. Y. Li, and K. Sarkar, Lateral migration of a capsule in plane shear near a wall, J. Fluid Mech. **739**, 421 (2014).

[40] R. K. Singh and K. Sarkar, Hydrodynamic interactions between pairs of capsules and drops in a simple shear: Effects of viscosity ratio and heterogeneous collision, Phys. Rev. E **92**, 063029 (2015).

[41] S. Mukherjee and K. Sarkar, Effects of matrix viscoelasticity on the lateral migration of a deformable drop in a wall-bounded shear, J. Fluid Mech. **727**, 318 (2013).

[42] S. Mukherjee and K. Sarkar, Effects of viscosity ratio on deformation of a viscoelastic drop in a Newtonian matrix under steady shear, J. Non Newtonian Fluid Mech. **160**, 104 (2009).

[43] K. Sarkar and W. R. Schowalter, Deformation of a two-dimensional viscoelastic drop at non-zero Reynolds number in time-periodic extensional flows, J. Non Newtonian Fluid Mech. **95**, 315 (2000).

[44] N. Aggarwal and K. Sarkar, Deformation and breakup of a viscoelastic drop in a Newtonian matrix under steady shear, J. Fluid Mech. **584**, 1 (2007).

[45] N. Aggarwal and K. Sarkar, Effects of matrix viscoelasticity on viscous and viscoelastic drop deformation in a shear flow, J. Fluid Mech. **601**, 63 (2008).

[46] N. Aggarwal and K. Sarkar, Rheology of an emulsion of viscoelastic drops in steady shear, J. Non Newtonian Fluid Mech. **150**, 19 (2008).

[47] S. Mukherjee and K. Sarkar, Viscoelastic drop falling through a viscous medium, Phys. Fluids **23**, 013101 (2011).

[48] S. Mukherjee and K. Sarkar, Lateral migration of a viscoelastic drop in a Newtonian fluid in a shear flow near a wall, Phys. Fluids **26**, 103102 (2014).

[49] G. I. Taylor, The formation of emulsions in definable fields of flow, Proc. R. Soc. London, Ser. A, **146**, 501 (1934).

[50] C. E. Chaffey and H. Brenner, A second-order theory for shear deformation of drops, J. Colloid Interface Sci. **24**, 258 (1967).

[51] S. Guido and M. Simeone, Binary collision of drops in simple shear flow by computer-assisted video optical microscopy, J. Fluid Mech. **357**, 1 (1998).

[52] V. Cristini, J. Bławzdziewicz, and M. Loewenberg, Drop breakup in three-dimensional viscous flows, Phys. Fluids **10**, 1781 (1998).